



HAL
open science

Post-translational acylation controls the folding and functions of the CyaA RTX toxin

Darragh P O'Brien, Sara E Cannella, Alexis Voegele, Dorothée Raoux-Barbot, Maryline Davi, Thibaut Douche, Mariette I Matondo, Sebastien Brier, Daniel Ladant, Alexandre Chenal

► To cite this version:

Darragh P O'Brien, Sara E Cannella, Alexis Voegele, Dorothée Raoux-Barbot, Maryline Davi, et al.. Post-translational acylation controls the folding and functions of the CyaA RTX toxin. 2021. pasteur-03221015

HAL Id: pasteur-03221015

<https://pasteur.hal.science/pasteur-03221015>

Preprint submitted on 7 May 2021

HAL is a multi-disciplinary open access archive for the deposit and dissemination of scientific research documents, whether they are published or not. The documents may come from teaching and research institutions in France or abroad, or from public or private research centers.

L'archive ouverte pluridisciplinaire **HAL**, est destinée au dépôt et à la diffusion de documents scientifiques de niveau recherche, publiés ou non, émanant des établissements d'enseignement et de recherche français ou étrangers, des laboratoires publics ou privés.



Distributed under a Creative Commons Attribution - NonCommercial 4.0 International License

1 **Post-translational acylation controls the folding and functions of the CyaA RTX toxin**

2 Darragh P. O'Brien^{1#}, Sara E. Cannella^{1#}, Alexis Voegele^{1,2}, Dorothée Raoux-Barbot¹,
3 Davi¹, Thibaut Douché³, Mariette Matondo³, Sébastien Brier^{1*}, Daniel Ladant^{1*} and
4 Alexandre Chenal^{1*}

5
6 **Addresses**

7 ¹ Institut Pasteur, Chemistry and Structural Biology Department, UMR CNRS 3528, 75724
8 PARIS cedex 15, France

9 ² Université Paris Diderot Paris VII, 75013 Paris, France

10 ³ Institut Pasteur, Proteomics Platform, Mass Spectrometry for Biology Unit, USR CNRS
11 2000, 75724 PARIS cedex 15, France

12

13 # these authors contributed equally to this work

14 * to whom correspondence and material requests should be addressed:

15 sebastien.brier@pasteur.fr; daniel.ladant@pasteur.fr; alexandre.chenal@pasteur.fr

16

17 **Keywords:** post-translational modification, acylation, protein folding, calcium-binding protein,
18 adenylate cyclase, bordetella pertussis, RTX motif

19

20 **Running title:** Acylation and calcium control CyaA folding

21

22

23 **List of abbreviations**

24 AC, N-terminal Adenylate cyclase Catalytic domain; cAMP, cyclic Adenosine
25 MonoPhosphate; CyaA, adenylate cyclase; HDX-MS, Hydrogen/Deuterium eXchange
26 followed by Mass Spectrometry; HR, Hydrophobic Region; PTM, Post-Translational
27 Modifications; pro-CyaA, non-acylated adenylate cyclase; RD, RTX Domain; RTX motif,
28 Repeat in ToXin motif; T1SS, Type 1 Secretion System; TR, Translocation Region;
29

30 **ABSTRACT**

31 CyaA is synthesized as a pro-toxin, pro-CyaA, and converted into its cytotoxic form upon
32 acylation of two lysines. After secretion, CyaA invades eukaryotic cells and produces cAMP,
33 leading to host defense subversion. To gain further insights into the effect of acylation, we
34 compared the functional and structural properties of pro-CyaA and CyaA proteins. HDX-MS
35 results show that the refolding process of both proteins upon progressive urea removal is
36 initiated by calcium binding to the C-terminal RTX domain. We further identified a critical
37 hydrophobic segment, distal from the acylation region, that folds at higher urea concentration
38 in CyaA than in pro-CyaA. Once refolded into monomers, CyaA is more compact and stable
39 than pro-CyaA, due to a complex set of interactions between domains. Our HDX-MS data
40 provides direct evidence that the presence of acyl chains in CyaA induces a significant
41 stabilization of the apolar segments of the hydrophobic domain and of most of the acylation
42 region. We propose a refolding model dependent on calcium and driven by local and distal
43 acylation-dependent interactions within CyaA. Therefore, CyaA acylation is not only critical
44 for cell intoxication, but also for protein refolding into its active conformation.

45

46 **Public Summary**

47 The contributions of post-translational modifications on the folding and activity of proteins
48 are still poorly understood. The adenylate cyclase toxin, CyaA, is a major virulence factor of
49 *Bordetella pertussis*, the causative agent of whooping cough. CyaA is produced as an inactive
50 pro-toxin, which is post-translationally acylated in the bacterial cytosol to yield the active
51 CyaA toxin, able to intoxicate human cells and induces cell death. Yet, the link between this
52 post-translational modification, the structure and the cytotoxic activities of CyaA remains
53 elusive. Here, using Hydrogen/Deuterium eXchange followed by Mass Spectrometry (HDX-
54 MS) and a combination of biophysical approaches, we demonstrate that acylation contributes
55 to the proper folding of CyaA into a compact and functional state. Our data sheds light on the
56 complex relationship between post-translational modifications, structural disorder and protein
57 folding. Coupling calcium-binding and acylation-driven folding is likely pertinent for other
58 Repeat-In-Toxin cytolysins produced by many Gram-negative bacterial pathogens.

59

60

61 INTRODUCTION

62 Post-translational modifications (PTM) are involved in the regulation of many cellular
63 processes and play a critical role in protein localization, structure, stability and function (1, 2).
64 Post-translational addition of acyl chains to bacterial toxins from the Repeat-In-Toxin (RTX)
65 family has been shown to be essential to their cytolytic activities. RTX toxins are calcium-
66 dependent virulence factors produced by various Gram-negative bacteria (3, 4). These
67 cytotoxins are synthesized as non-active precursors that require “activation” by selective post-
68 translational acylation carried out by dedicated acyltransferases that use an acyl-acyl carrier
69 protein (acyl-ACP) as fatty acid donor (5-9). Once acylated, the RTX toxins are secreted *via*
70 dedicated type 1 secretion systems (T1SS) and exert their virulence on a variety of target cells
71 (10). Most are cytolysins endowed with a pore-forming activity that alter the membrane
72 integrity of their target cells (3, 4, 11) while few others have additional cytotoxic activities
73 (see below). How the acyl chains regulate the biological activities of these RTX cytolysins
74 has remained elusive thus far.

75 Here we address this question by exploring the effects of post-translational acylation
76 on the structure and functions of the adenylate cyclase toxin (CyaA) from *Bordetella pertussis*,
77 the causative agent of whooping cough (12). In addition to its pore-forming activity, CyaA
78 possesses an extra domain endowed with adenylate cyclase activity. This AC domain is
79 delivered into the cytoplasm of target cells (13, 14) where it is activated by calmodulin (15,
80 16), to produce high levels of cAMP, subverting host immunity (10, 17, 18). CyaA is a large,
81 multi-domain protein of 1706 amino acid residues (Figure 1), with an N-terminal adenylate
82 cyclase catalytic domain, AC, (residues 1-364) (16), while the C-terminal hemolysin region
83 (residues 365-1706) contains several domains responsible for AC membrane translocation and
84 pore-forming activity (19-24). The translocation region, TR, (residues 365-527) is involved in
85 AC translocation across target cell membranes (24), membrane permeabilization (25) and
86 exhibits features similar to membrane-active peptides (24, 26, 27). The hydrophobic region,
87 HR, corresponds to residues 528 to 710 while the acylation region, AR, extends from residues
88 711 through 1005. CyaA is synthesized as an inactive precursor, pro-CyaA, that is converted
89 into its active form upon specific acylation of two lysine residues (Lys 860 and Lys 983) by
90 CyaC, an acyltransferase that catalyzes the transfer of an acyl chain from an acyl-ACP (acyl-
91 carrier protein) to the epsilon-amino groups of pro-CyaA lysines (7, 28-30). Finally, the C-
92 terminal 701 residues (1006-1706) correspond to the cell receptor-binding domain, RD, which
93 harbors ~40 copies of a glycine and aspartate rich nona-peptide repeat, characteristic of the
94 RTX bacterial cytolysins. In the absence of calcium, these RTX motifs are intrinsically
95 disordered, but undergo a disorder-to-order transition upon calcium binding (4, 31-42). The
96 RTX motifs themselves constitute the primary sites of calcium binding within the protein (3,
97 31, 43, 44).
98 It is well known that acylation is critically required for the pore-forming activity of CyaA as
99 well as its ability to invade cells to produce high levels of cAMP (*i.e.*, cell intoxication) (45,
100 46). Here, we have analyzed the structural and hydrodynamic properties of both pro-CyaA

101 and CyaA monomers to provide insights into their folding process, and to identify the
102 structural basis of the acylation-dependent gain of functions. Our biophysical data show that
103 the acylated CyaA protein adopts a more compact and stable monomeric state than pro-CyaA,
104 while Hydrogen/Deuterium eXchange followed by Mass Spectrometry (HDX-MS) studies
105 provided direct evidence of long-range interactions between the hydrophobic and acylation
106 regions. HDX-MS results further indicate that these interactions are strongly favored in the
107 presence of the acyl chains. We propose that these interactions may directly contribute to the
108 folding of the acylated CyaA protein into a compact and functional monomeric state. Our data
109 indicates that calcium-binding and post-translational acylation play a key role in the folding
110 of CyaA into its cytotoxic form.
111

112 MATERIALS AND METHODS

113 *Overexpression and purification of pro-CyaA and CyaA in urea and production of the* 114 *monomeric species*

115 Buffer A was composed of 20 mM Hepes, 150 mM NaCl, pH 7.4. Production and
116 purification of pro-CyaA and CyaA, and refolding of both species into holo-monomers was
117 performed as previously described (41, 47). The pro-CyaA urea stock solution was loaded at 2
118 μM (compared to 5 μM for CyaA) on a size exclusion chromatography column (HiLoad
119 26/600 Superdex 200 pg, average particle size: 34 μm ; column dimensions: 26*600 mm or
120 Superdex 200 Increase 10/300 GL, average particle size: 8.6 μm ; column dimensions: 10*300
121 mm or Agilent BioSEC-5, particle size: 5 μm , pore size: 300Å, column dimensions: 21.2*300
122 mm) to refold the protein into a monomeric species. The monomer-to-multimer ratio
123 increases as the particle size decreases.

124 *Identification of the post-translational acylation of pro-CyaA and CyaA by mass* 125 *spectrometry*

126 *Protein digestion.* CyaA (9 μM) and pro-CyaA (7 μM) in 6 M urea buffer were firstly
127 digested with Lys-C (#V1671, Promega) at a Lys-C/toxin ratio of 1/50 (w/w), at 37°C for 3h.
128 To ensure optimal trypsin activity, the urea concentration was decreased below 2 M with
129 addition of 2 volumes of buffer A, then a second digestion was performed with Trypsin
130 (Sequencing Grade Modified Trypsin #V5111, Promega) at a enzyme/toxin ratio of 1/50
131 (w/w) at 37°C for 1h. Digestion was stopped by adding formic acid to 2% final concentration.
132 Digested peptides were desalted and concentrated with C18 Spin Columns Pierce™
133 (ThermoFisher Scientific - 89870) according to manufactures instructions. Peptides were
134 vacuum centrifuged and then lyophilized. Peptides were reconstituted in 2% ACN / 0.1% FA.
135 LC-MS/MS analysis. A Proxeon EASY-nLC 1000 nanochromatographic system (Thermo
136 Fisher Scientific, Bremen) was coupled on-line to a LTQ-Orbitrap Velos Mass Spectrometer
137 (Thermo Fisher Scientific, Bremen). For each sample, 0.5 μg of peptides was directly loaded
138 onto a 15 cm home-made C4 column (5 μm particles, 300 Å pore size, ReproSil-Pur 300 C4,
139 Dr. Maisch GmbH, Ammerbuch-Entringen, Germany) and eluted by a one step gradient from
140 3.0% to 80% solvent B (80 % ACN, 0.1 % FA) in 50min, at a flow rate of 250 nL/min. MS
141 data was acquired using Xcalibur software with a survey scan (100-1800 m/z) analyzed into
142 the Orbitrap mass analyzer at a resolution setting of 60,000 followed by 15 CID
143 fragmentations analyzed in the linear ion trap. The AGC* target for MS and MS/MS scans
144 were set to 1E6 and 5E3 respectively. The isolation width was set to 2.5 m/z and the
145 normalized collision energy was set to 35. Selected ions were dynamically excluded for 15
146 sec.

147 *Data analysis.* All raw data was analyzed using MaxQuant software version 1.5.1.2
148 (48) and the Andromeda search engine (49). Based on the protein expression system, data was
149 searched against the complete *E. coli* strain K12 UniProt database (4,331 proteins,
150 downloaded 2015-10-08), and CyaA protein sequence. The digestion mode was set to trypsin,
151 and a maximum of two missed cleavages were allowed. Carbamidomethylation of cysteine

152 was specified as a fixed modification. Variable modifications considered were N-terminal
153 acetylation, oxidation of methionines and N-acylation of lysines (Myristoyl-4H,
154 Myristoleylation, Myristoylation, Palmitoleylation, Palmitoylation). The minimum peptide
155 length was fixed to 5 amino acids and the required false discovery rate was set to 1% at the
156 peptide spectrum match (PSM) and protein level. The main search peptide tolerance was set
157 to 4.5 ppm and to 0.5 Da for the MS/MS match tolerance. Second peptides were enabled to
158 identify co-fragmentation events. Results of PTM identification are shown in Supplemental
159 Figures S2A-C.

160 ***HDX-MS of pro-CyaA and CyaA conformation and dynamics***

161 We used Hydrogen/Deuterium eXchange followed by Mass Spectrometry (HDX-MS)
162 to characterize the refolding process of pro-CyaA and CyaA equilibrated in 6, 3 or 1.6 M urea,
163 as well as the monomeric species in the complete absence of denaturant. Two experimental
164 conditions were analyzed; *A*: to monitor the effect of post-translational acylation on the
165 refolding process of full-length pro-CyaA and CyaA at 6 M, 3 M and 1.6 M urea, and *B*: to
166 determine the effect of acylation on the full-length pro-CyaA and CyaA monomers. To
167 achieve this, several proteins and conditions were analyzed; firstly, pro-CyaA and CyaA each
168 in the presence of 6, 3 and 1.6 M urea containing either 2 mM CaCl₂ or 2 mM EDTA, and
169 secondly, fully-folded pro-CyaA and CyaA monomers in buffer A, complemented with 2 mM
170 CaCl₂.

171 *HDX-MS sample preparation.* Prior to addition of the deuterated buffer (100% D₂O in
172 20 mM Hepes, 150 mM NaCl, pH 7.4, supplemented or not with 6 M, 3M or 1.6 M urea), all
173 solutions were equilibrated for 1 h at 20°C. For experiment A, labeling was initiated by
174 diluting each sample five-fold with the deuterated buffer and incubated for $t = 0.16, 1, 10, 60,$
175 and 240 min at 20°C (final protein concentration of 0.3 μ M during labeling); experiment B
176 was performed using a final protein concentration of 1 μ M and identical labeling conditions
177 for $t = 0.16, 0.5, 1, 5, 10, 30, 60, 120, 240, 480$ and 1440 min, respectively.

178 The 80% excess of deuterium reached during labeling ensured unidirectional exchange.
179 Aliquots of 3-10 pmol of protein were withdrawn at each experimental time point and
180 quenched upon mixing of the deuterated sample with ice-cold 0.5% formic acid solution to
181 achieve a final pH of 2.5. For experiment A (in the presence of urea), the quench was
182 performed by mixing 14 mL of labeled sample with 56 mL of ice cold 0.5% formic acid (ratio
183 1/5: v/v, final H₂O/D₂O ratio = 20%/80%). For experiment B (monomeric species), the quench
184 was performed by mixing 30 mL of labeled sample with 30 mL of ice cold 0.5% formic acid
185 (ratio 1/2: v/v, final H₂O/D₂O ratio = 50%/50%). Quenched samples were immediately snap-
186 frozen in liquid nitrogen and stored at -80°C for approximately 12 h. Undeuterated controls
187 were treated using an identical procedure. Triplicate independent technical analyses were
188 performed for each time point and condition for all HDX-MS analyses.

189 *HDX-MS data acquisition.* Prior to MS analysis, samples were rapidly thawed. To
190 minimise back exchange, the LC solvent line, injection valve, and sample loop were
191 maintained at 0°C. To achieve this, local HDX analyses were performed with the aid of a

192 cooled HDX Manager (Waters Corporation, Milford, MA). Samples were digested using an
193 in-house prepared cartridge of immobilized pepsin beads (Thermo Scientific, Rockford, IL),
194 for 2 min at 70 $\mu\text{L}/\text{min}$ and 20°C. Peptic peptides were rapidly desalted and concentrated
195 using a Vanguard C18 pre-column (1.7 μm , 2.1 x 5 mm; Waters Corporation), and separated
196 using an ACQUITY UPLC™ BEH C18 column (1.7 μm , 1 x 100 mm). Pro-CyaA and CyaA
197 peptides were separated over a 10 min gradient of 5-40% ACN at 38 $\mu\text{L}/\text{min}$ and at 0°C. The
198 LC flow was directed to a Synapt™ G2-Si HDMS™ mass spectrometer (Waters), which was
199 equipped with ESI and lock-mass correction using Glu-Fibrinogen peptide. Mass spectra were
200 acquired in positive-ion mode over the m/z range of 50–1800 using a data-independent
201 acquisition scheme (MS^E) whereby exact mass information is collected at both low and high
202 collisional energies for collisional induced dissociation. Unlabeled pro-CyaA and CyaA
203 samples were digested in triplicate to build a peptide coverage map.

204 *HDX-MS data processing.* Peptide identification was *via* the Protein Lynx Global
205 Server (PLGS) 3.0 (Waters Corporation). Oxidation of methionines and carbamylation of N-
206 terminal and lysine residues were set as variable modifications. The sequence coverage map
207 (Supplemental Figures S3 and S4) was plotted using DynamX 3.0 HDX software (Waters).
208 For the native proteins, pepsin digestion yielded 232 unique peptides identified from their
209 accurate masses and product ion spectra. A total of 141 peptides were brought forward for
210 HDX data analysis, corresponding to a sequence coverage of 91.0%. For the proteins in urea,
211 172 peptides, covering 85.7% of the protein sequence, were selected for final analysis. The
212 reduced sequence coverage witnessed here was due to the experimental design necessitating a
213 lower protein load on column at the 1.6 M urea concentration (down to 3 pmol, in contrast to
214 10 pmol for all other states), resulting in a knock-on decrease in MS sensitivity. D₂O uptake at
215 the peptide level was extracted and visualized in uptake charts, difference plots, and heat
216 maps, performed in both DynamX and MEMHDX (50). Statistical analysis of HDX-MS
217 results was performed with MEMHDX (Wald test, false discovery rate sets to 1%).

218 *Urea unfolding of pro-CyaA and CyaA monomers*

219 A volume of 2.5 μL of CyaA or pro-CyaA monomers stored in 20 mM Hepes, 150
220 mM NaCl, 2 mM CaCl₂, pH 7.5 was diluted in 20 mM Hepes, 150 mM NaCl, 2 mM CaCl₂,
221 containing urea at various concentrations to obtain a final concentration of toxin of 50 nM. A
222 total of 22 tubes were prepared, with a urea gradient from 0 to 6 M. Once diluted, the toxin
223 was incubated at room temperature for 1 h. Emission spectra of the protein were acquired on a
224 Jasco FP 8200 spectrofluorimeter (Jasco, Tokyo, Japan) using a 3 x 3 mm path length quartz
225 cell (105.251.QS, Hellma Analytics). The excitation wavelength was set to 280 nm, both
226 emission and excitation slits were fixed at 5 nm, and fluorescence emission spectra were
227 recorded from 300 to 400 nm. Spectra were acquired at 25°C. The ratio of fluorescence
228 intensities at 340 and 380 nm were plotted against the urea concentration.

229 *ANS binding to CyaA and pro-CyaA monomers*

230 Freshly prepared ANS was added to pro-CyaA or CyaA monomers to reach final

231 concentrations of 5 and 0.5 μM , respectively (molar ratio of ANS:toxin was 10:1). Excitation
232 was fixed at 360 nm and emission spectra were recorded between 400 and 600 nm on a Jasco
233 FP 8200 spectrofluorimeter (Jasco, Tokyo, Japan) using either a 3 x 3 mm path length quartz
234 cell (105.251.QS, Hellma Analytics) or a 10 μL drop cell. All spectra were acquired at 25°C.

235 ***Analytical ultracentrifugation (AUC) analysis of pro-CyaA and CyaA monomers***

236 Sedimentation velocity experiments were performed on a Beckman XL-A analytical
237 ultracentrifuge (Beckman Coulter) in a AN60-Ti rotor at 20 °C. All samples were filtered on
238 0.2 μm filters before experiments. Detection of the protein concentration as a function of
239 radial position and time was performed by optical density measurements at a wavelength of
240 280 nm. For sample analysis, 400 μL of pro-CyaA or CyaA at 1 μM was loaded into a 1.2
241 mm-thick two-channel epoxy centerpiece and spun at 20,000 rpm. Data were analyzed with
242 SEDFIT software using a continuous size distribution c(s) model (15, 41, 51).

243 ***Hemolysis of erythrocytes***

244 The hemolytic activity of pro-CyaA and CyaA was determined on sheep erythrocytes
245 as previously described (47). Briefly, sheep erythrocytes were washed several times with
246 buffer A and resuspended at 5×10^8 cells/mL. The hemolytic activity of pro-CyaA and CyaA
247 was measured after overnight incubation of erythrocytes at 37 °C by quantifying the amount
248 of hemoglobin released at 540 nm (and of intracellular content release at 405 nm).

249 ***Pro-CyaA and CyaA translocation and cAMP production in erythrocytes***

250 The invasive activity of CyaA was determined by measuring the intracellular cAMP
251 accumulation as previously described (47). Briefly, erythrocyte suspensions (5×10^8 cells/mL
252 in buffer A) were incubated with 5.6 nM CyaA ($1 \mu\text{g} \cdot \text{mL}^{-1}$) at 37 °C for 20 min. The cells
253 were washed and lysed as described (41) and then the intracellular cAMP content was
254 determined by a homemade competitive ELISA immunoassay (52) using a rabbit anti-cAMP
255 antiserum (1818-II) and a goat anti-rabbit IgG coupled to alkaline phosphatase (Sigma, Life
256 Science). The alkaline phosphatase activities were revealed with 4-Nitrophenyl phosphate
257 disodium salt hexahydrate (PA substrate from Sigma, Life Science) and cAMP concentrations
258 were calculated from a standard curve established with known concentrations of cAMP
259 diluted in buffer A.

260 ***Data availability***

261 All data generated and analyzed during this study are included in this published article and its
262 supplemental information files.

263

264 **RESULTS**

265 ***Production and MS characterization of CyaA and pro-CyaA***

266 Pro-CyaA and CyaA were overexpressed in *E. coli* - the latter by co-expression of pro-
267 CyaA and CyaC (53-55) – and purified to homogeneity using established methods (47). To
268 identify the acyl chains incorporated in CyaA, the pro-CyaA and CyaA proteins were digested
269 by Lys-C and trypsin and analyzed by MS. Two peptides (858-872 and 972-984) containing
270 the K860 and K983 residues were identified. Both residues were primarily palmitoleylated
271 (C16:1) in CyaA (see Supplemental Figures S1A-C). Palmitoylation (C16:0) was also
272 identified on both K860 and K983 residues. Traces of myristoylation (C14:0) were observed
273 on K983. As expected, no acylation was detected on K860 or K983 in pro-CyaA. In summary,
274 CyaA is primarily post-translationally modified with C16 acyl chains on both lysines, while
275 pro-CyaA is devoid of the PTM.

276 ***Refolding and functional activities of CyaA and pro-CyaA***

277 Due to their size and hydrophobic character, both pro-CyaA and CyaA proteins are
278 prone to aggregation. They are traditionally purified in the presence of chaotropic agents
279 (usually urea) and stored in an unfolded state in denaturing conditions (*i.e.*, 6-8 M urea).
280 Upon refolding by urea dilution, mixtures of multimeric and monomeric species are
281 commonly obtained, precluding further biochemical and biophysical characterization (41).
282 Yet, we have recently achieved to refold both pro-CyaA and CyaA into monomeric states (see
283 Supplemental Figure S2) that remain stable in the absence of urea (41, 47), thus allowing us
284 to investigate the relationship between the structure and function of these two species. The
285 method is based on molecular confinement to prevent intermolecular interactions between
286 hydrophobic regions of proteins upon their refolding. Refolding is performed on a size-
287 exclusion chromatography column used as molecular confinement media comprising a matrix
288 characterized by small size particles (see methods for details and Supplemental Figure S2). In
289 addition to the monomeric species, this refolding procedure also leads to the formation of a
290 heterogeneous population of CyaA multimers. We have previously observed that beside
291 molecular confinement, refolding is critically dependent on the presence of calcium and toxin
292 acylation (41, 47). However, we succeeded to refold pro-CyaA into a monomeric protein by
293 optimizing the procedure, essentially by decreasing the initial protein concentration, although
294 the recovery yield was low as compared to that of acylated CyaA (see Supplemental Figure
295 S2 and methods for details).

296 The biological activities of the refolded pro-CyaA and CyaA species were assessed on
297 sheep erythrocytes by monitoring hemolytic activity and the ability of the toxins to invade
298 cells (Supplemental Table S1). As expected, the monomeric CyaA species induced hemolysis
299 and was able to bind to erythrocytes and translocate into the cytosol in a calcium-dependent
300 manner, in agreement with prior studies (25, 47, 55, 56). In contrast, the multimeric CyaA
301 species exhibited strongly reduced hemolytic activity and was not able to translocate into
302 erythrocytes while the pro-CyaA species were totally lacking hemolytic and cell invasion
303 capacities (Supplemental Table S1) in agreement with previous studies (53, 57). This

304 confirms that the monomeric, acylated CyaA is the physiological competent state of the toxin,
305 able to invade eukaryotic target cells.

306 ***Compactness and solvent-exposed hydrophobic regions in CyaA and pro-CyaA***

307 We then characterized the biophysical and hydrodynamic properties of pro-CyaA and
308 CyaA. We first determined the compactness and stability of both proteins using macroscopic
309 approaches, and then characterized the proteins at medium resolution by HDX-MS. The
310 solvent-exposed hydrophobic surfaces of pro-CyaA and CyaA monomers were probed using
311 ANS fluorescence (58) in buffer A, complemented with 2 mM CaCl₂. While a slight increase
312 in ANS fluorescence intensity was observed in the presence of CyaA monomers, a marked
313 increase (approximately 3-fold) was found with the pro-CyaA monomers, suggesting that
314 these latter expose more hydrophobic regions to the solvent than the former (Figure 2A). In
315 other words, the hydrophobic regions in CyaA monomers are less accessible to ANS than
316 those in the pro-CyaA species, suggesting that acylation favors the shielding of hydrophobic
317 regions within the protein. We then investigated the compaction state of CyaA and pro-CyaA
318 by sedimentation velocity analysis using AUC. Both species remain essentially monomeric,
319 with only a few aggregates observed on the time scale of the experiment (Figure 2B). The
320 analysis provided a sedimentation coefficient of 7.4 and 7.1 S, respectively, for CyaA and
321 pro-CyaA monomers (Figure 2B and Supplemental Table S2), suggesting that pro-CyaA
322 monomers are slightly less compact than CyaA monomers. We further compared the stability
323 of pro-CyaA and CyaA monomers by following their urea induced unfolding by intrinsic
324 tryptophan fluorescence. The denaturation data also indicate that CyaA is more stable than
325 pro-CyaA at urea concentrations above 2 M (Figure 2C) as highlighted by the plot of the
326 maximum wavelength differences between the two proteins (Figure 2D). Taken together,
327 these results indicate that pro-CyaA monomers expose more hydrophobic regions to the
328 solvent (Figure 2A), and are less compact (Figure 2B) and stable (Figures 2C-D) than CyaA
329 monomers.

330 ***HDX-MS analysis of the pro-CyaA and CyaA refolding process***

331 To further characterize the refolding process of pro-CyaA and CyaA, we used HDX-
332 MS to probe the structure and dynamics of both full-length proteins equilibrated in 6, 3 or 1.6
333 M urea, as well as the monomeric species in the complete absence of denaturant. Figure 3
334 displays a global view of the relative deuterium fractional uptake of CyaA equilibrated in 6, 3
335 or 1.6 M urea in the presence of 2 mM CaCl₂. The relative fractional exchanges of three
336 independent replicates were calculated for each peptide at each time point and plotted as a
337 function of peptide position (CyaA peptide maps are shown in figures S3 and S4). In 6 M urea
338 (Figure 3B), the protein is totally devoid of dynamic HDX-MS events, confirming that CyaA
339 is completely denatured. In 3 M urea (Figure 3C), a short segment of the hydrophobic region
340 (658-719 in HR) and a large part of the RTX domain (RD, from Block II to the C-terminal
341 extremity of CyaA) exhibit dynamic HDX-MS behavior, while in 1.6 M urea (Figure 3D),
342 part of the catalytic domain (the T25 region of AC), AR and most of HR also has dynamic
343 HDX-MS activity. These results suggest that these regions of CyaA sequentially acquire

344 structural elements upon progressive urea removal. This sequential folding of CyaA is further
345 highlighted in Supplemental Figure S5. To identify the contributions of calcium on CyaA
346 refolding, similar HDX-MS experiments were repeated in the absence of calcium
347 (Supplemental Figure S6). In these conditions, the entire CyaA polypeptide remains solvent
348 accessible and unfolded at all urea concentrations, even down to 1.6 M. The uptake difference
349 plots between CyaA samples in the presence of calcium or EDTA at various urea
350 concentrations are compared in Figure 4 (and Supplemental Figures S7-S9 for a detailed
351 presentation of the HDX-MS data). These HDX-MS results show that the presence of calcium
352 is critical for the acquisition of structural elements in CyaA at 3 M and 1.6 M urea. This
353 further indicates that calcium binding to the RTX motifs is critical not only to induce folding
354 of the C-terminal RD domain (see the effect of calcium versus EDTA at 3 M urea in Figure
355 4C), but also for the structuration of all of the upstream N-terminal domains of CyaA (see the
356 effect of calcium versus EDTA at 1.6 M urea in Figure 4D).

357 Similar HDX-MS experiments were also performed on pro-CyaA (Supplemental
358 Figure S10) and revealed a comparable sequential refolding process with RD acquiring
359 structures at intermediate urea concentrations (3 M), followed by the refolding of AC and HR
360 regions at lower urea concentrations (1.6 M) (Supplemental Figures S10 and S11). As in
361 CyaA, several regions of pro-CyaA display non-dynamic HDX-MS throughout, indicating
362 that these regions remain largely unstructured, even at low urea concentrations. These include
363 a large stretch of amino acids from the C-terminal end of the catalytic domain (T18 fragment),
364 across the translocation region, TR, and through the N-terminal part of HR, *i.e.*, from residues
365 345 to 570. Similarly, residues 821 through 981 of the AR domain show non-dynamic HDX-
366 MS behavior throughout. Significant differences do exist between the acylated and non-
367 acylated proteins, however, as illustrated in Figure 5, which shows the difference in deuterium
368 uptake between pro-CyaA and CyaA at both 3 M and 1.6 M urea. In 3 M urea (Figure 5B),
369 the differences are confined to a segment of the HR between amino acids 658 and 719. In 1.6
370 M urea (Figure 5C), further minor structural disparities between pro-CyaA and CyaA are
371 evidenced, extending upstream from the HR to the TR region, through to the N-terminal part
372 of AC, and, conversely, downstream, to the AR region. It therefore seems that the acyl chains
373 at K860 and K983 of CyaA are critically involved in the folding of the segment encompassing
374 residues 658 to 719 (Figures 5B-C). We propose that the hydrophobic effects between the
375 acyl chains and HR restrict the conformational landscape of CyaA, thus favoring a faster
376 refolding towards the folded state, as compared to pro-CyaA. The present data suggests that
377 the segment covering residues circa 660-710 of the HR can act as a hydrophobic folding
378 nucleus, even in the presence of 3 M urea if K860 and K983 are acylated (Figures 3 and 5C).
379 In pro-CyaA, this hydrophobic collapse occur at lower urea concentrations due to the lack of
380 acyl chains (Figure S11), and consequently, the partially folded hydrophobic regions may
381 remain exposed to the solvent, thereby favoring the aggregation of pro-CyaA into multimeric
382 species.

383 The relative fractional uptake maps of monomeric pro-CyaA and CyaA species (both
384 in the absence of urea) are displayed in Figure 6. Extensive dynamic HDX-MS activity,
385 indicative of secondary structural elements, is observed throughout both proteins. Yet,
386 segments that connect individual sub-domains, such as at the boundary of the AC/TR, HR/AR,
387 and AR/RD domains, appear to be more accessible than the adjacent domains. Equivalent
388 HDX-MS patterns are observed between several domains of pro-CyaA and CyaA monomers
389 as illustrated in the uptake difference plot (Figure 6D), in particular the N-terminal parts of
390 both AC and TR, and the blocks III to V of RD. These data suggest that the folding of these
391 regions is not affected by CyaA acylation. The C-terminal part of TR (circa 454-520) and the
392 N-terminal part of RD (mainly blocks I and II) are weakly but significantly stabilized by the
393 presence of the acyl chains (Figure 6D).

394 The strongest differences in HDX-MS activity between the two forms of CyaA are
395 found in the hydrophobic and acylation regions (Figures 6D-E). Firstly, peptides from the AR
396 region (i.e. residues between amino acids 798 and 958), appear to be more solvent accessible
397 in pro-CyaA monomer than in the monomeric CyaA toxin (Figures 6B and 6C, respectively).
398 Secondly, significant changes in HDX-MS patterns are observed in the hydrophobic region of
399 CyaA, most notably at peptides 539-546, 571-582, 615-622, 658-672, 682-696 and 686-696
400 (highlighted in Figures 6D, 6E and S12), corresponding to the four hydrophobic segments of
401 HR (Supplemental Figures S12 and S13). Interestingly, a significant difference in HDX-MS
402 activity is observed in all experimental conditions between pro-CyaA and CyaA for the
403 hydrophobic segment between amino acids 660 and 710 (Figures 5B-C, 6 and S13). This
404 confirms that these hydrophobic segments may indeed play an essential role in the folding
405 process of the acylated toxin, from the initial structural elements observed at 3 M urea
406 (Figures 3 and 5) to the native state of the monomeric CyaA (Figure 6). The HDX-MS data
407 provides direct evidence that CyaA acylation favors a hydrophobic collapse of these regions
408 that may constitute the apolar core of the protein structure.

409

410 **DISCUSSION**

411 Acylation is a requisite PTM for the cytotoxicity of RTX toxins, but the precise
412 contribution of acyl chains to the structure and function of these cytolysins still remains
413 largely unknown. We previously suggested that acylation may play a crucial role in the
414 refolding of the *B. pertussis* adenylate cyclase toxin, CyaA, a prominent member of the RTX
415 toxin family, into a monomeric and functional species (41, 47). To gain further insights into
416 the effect of CyaA acylation, we directly compared the biophysical and functional properties
417 of the monomeric acylated and non-acylated forms (CyaA and pro-CyaA, respectively) of this
418 toxin.

419 MS analysis indicates that CyaA produced in *E. coli* in the presence of the CyaC
420 acyltransferase is mainly modified by C16 acyl chains on K860 and K983, and, as expected,
421 pro-CyaA is not. AUC experiments demonstrate that CyaA monomers are more compact than
422 their pro-CyaA counterparts, while ANS binding studies show that hydrophobic regions are

423 less solvent-exposed in CyaA than in pro-CyaA. This indicates that the presence of acyl
424 chains in CyaA may favor a more compact structural state. Furthermore, urea-induced
425 unfolding experiments suggest that the acylated toxin is more stable than pro-CyaA. All
426 together, our AUC and fluorescence data shows that several hydrophobic regions may be
427 more solvent-exposed in pro-CyaA than CyaA, leading to a less compact and stable protein.

428 We exploited HDX-MS to unravel the folding process of both pro-CyaA and CyaA by
429 analyzing their structural dynamics at different urea concentrations. These studies lead to two
430 important conclusions. Firstly, we show that in both forms of the protein, *i.e.*, independently
431 of the acylation-status, the C-terminal RTX-containing domain RD is the first region to
432 acquire structure when the refolding is carried out in the presence of calcium (Figures 3, 4 and
433 S5-11). More importantly, we found that in the absence of calcium the entire protein remains
434 essentially unstructured even after lowering urea concentrations down to 1.6 M urea, as
435 indicated by the absence of any significant solvent-protection across the entire CyaA
436 polypeptide chain (Figures S6-S9 and 4D). In marked contrast, in the presence of calcium,
437 most CyaA domains do contain structural elements at 1.6 M urea and in the absence of urea,
438 as evidenced by HDX-MS (Figures 3D, 4D, 6C, S5A and S9). Our previous studies already
439 established that the RTX domain of CyaA, RD, (residues 1006-1706) is intrinsically
440 disordered in the calcium-free apo-state and folded in the calcium-bound holo-state (4, 31-39,
441 41, 42, 59). A likely scenario is that, in the absence of calcium, the intrinsically disordered
442 nature of RD within the full-length protein may result in a huge entropic penalty that prevents
443 folding of the other CyaA domains. This data has direct implications for CyaA secretion. We
444 previously suggested that in the low calcium environment of the bacterial cytosol, RD adopts
445 disordered conformations favorable for transport through the type 1 secretion machinery, and
446 folds upon binding calcium in the extracellular, calcium-rich environment (4, 32, 34, 39, 41,
447 42). Our present data now extends this model to the full-length CyaA toxin. Indeed, our
448 HDX-MS results clearly indicate that in the low calcium environment of the bacterial
449 cytoplasm, it is not only the RD domain, but the CyaA polypeptide chain as a whole, that
450 preferentially adopts unstructured conformations that fosters protein secretion through the
451 type 1 secretion channel. Upon secretion, as the protein reaches the calcium-rich extracellular
452 medium, RD binds calcium, folds, and may then act as a scaffold for the refolding of the
453 upstream domains of CyaA that are progressively exiting the T1SS machinery in a C- to- N-
454 terminal vectorial secretion process (39-41).

455 The second major finding of this study is that acylation plays a critical role in the
456 folding of CyaA into a functional cytotoxic state. HDX-MS revealed dramatic differences in
457 deuterium uptake between the acylated and non-acylated CyaA, mainly located in the
458 hydrophobic and acylation regions (Figures 5, 6, S5, S11 and S12). More specifically, we
459 identified a segment (circa residues 660-710) within the hydrophobic region and distal from
460 the acylation sites, which appears to play a central role in toxin refolding (Figures 5B-C). We
461 propose that in CyaA, this region may directly interact and collapse with the distant acyl
462 chains, in a process driven by hydrophobic effects. The formation of these structural elements

463 may orient the initial CyaA folding pathway and favor toxin refolding into the monomeric
464 state. In contrast, pro-CyaA may have to explore a broader conformational landscape due to
465 the absence of the initial hydrophobic collapse between residues 660-710 and the acyl chains.
466 Thus, from a kinetic point of view, the acyl chains may favor a faster folding of CyaA as
467 compared to pro-CyaA. This could also explain the higher propensity of pro-CyaA to
468 aggregate, and consequently the lower yield of pro-CyaA monomers compared to CyaA
469 during the refolding process (Supplemental Figure S2).

470 We propose the following calcium- and acylation-dependent refolding scheme for
471 CyaA: as CyaA exits from the T1SS, calcium-binding triggers refolding of the C-terminal
472 RTX domain. As previously proposed, the calcium-loaded, folded RTX domain might act as a
473 scaffold for the folding of other CyaA domains, i.e., AR and HR (Figures 3, 4 and S7-S9).
474 The acyl chains attached to K860 and K983 foster a hydrophobic collapse within the apolar
475 segment spanning residues 660-710 (Figures 5 and S13), which acts as a nucleus for the
476 folding into the native state (Figure 6D) of both HR (residues 528-710) and AR (711-1005).
477 Finally, TR and AC are secreted and, interestingly, their folding appears minimally affected
478 by the acylation status. This is in agreement with the fact that the isolated AC and AC-TR
479 polypeptides can autonomously fold in solution (15, 16, 24). Taken together, the calcium-
480 induced folding, coupled with hydrophobic effects between distal regions containing apolar
481 segments and acyl chains, is likely shared with other multi-domain proteins. This is probably
482 the case of other large RTX cytolytins like CyaA, which are secreted in an unfolded state and
483 refold in the host environment to exert their virulence (3, 4).

484

485 **ACKNOWLEDGEMENTS**

486 D.O.B was supported by PasteurInnov2015-197 and PTR451 grants. S.E.C. was supported by
487 a stipend from the Pasteur - Paris University (PPU) International PhD Program. A.V. was
488 supported by a DIM MalInf (infectious diseases) grant. We thank Bertrand Raynal and
489 Sébastien Brulé from the PFBMI for their excellent technical expertise with AUC. Running
490 costs were supported by Institut Pasteur, PasteurInnov (PIV15-197), PTR grant (PTR451),
491 CNRS, Fondation Recherche Médicale (FRM DBS20140930771). We thank the CACSICE
492 Equipex ANR-11-EQPX-0008.

493

494 **AUTHOR CONTRIBUTIONS**

495 A.C. designed the project. D.O.B., T.D., M.M., S.B., and A.C. designed the experiments.
496 D.O.B., S.E.C., A.V., M.D., T.D., S.B., and A.C. performed the experiments. D.O.B., S.E.C.,
497 T.D., M.M., S.B., D.L. and A.C. analyzed the data. D.O.B., S.E.C., S.B., D.L., and A.C.
498 wrote the manuscript. All authors discussed the results and commented on the manuscript.

499

500 **DECLARATION OF INTERESTS**

501 The authors declare no competing interests.

502

503 **SUPPLEMENTAL INFORMATION**

504 The Supplemental Information file contains 13 Supplemental Figures and 2 Supplemental
505 Tables.

506

507

508 **FIGURE TITLES AND LEGENDS**

509 **Figure 1: Schematic representation of the multi-domain CyaA toxin (1706 amino acid**
510 **residues).** The toxin contains the following domains: a N-terminal adenylate cyclase catalytic
511 domain (AC, residues 1-364), a translocation region (TR, residues 365-527), a hydrophobic
512 region (HR, residues 528 to 710), an acylation region (AR, residues 711-1005 with acylated
513 Lys 860 and Lys 983 marked with yellow stars), and a C-terminal RTX domain (RD, 1006-
514 1706), composed of five consecutive blocks.

515

516 **Figure 2: Macroscopic characterization of CyaA and pro-CyaA monomeric species.**
517 Panel A shows the emission fluorescence spectra of ANS in the absence (black) and in the
518 presence of CyaA (blue) and pro-CyaA (red) monomers. Panel B shows the distribution of
519 sedimentation coefficients $c(s)$ of CyaA (blue) and pro-CyaA (red) monomers measured by
520 analytical ultracentrifugation (AUC). The AUC data are presented in Supplemental Table S2.
521 Panel C shows the urea-induced unfolding of CyaA (blue) and pro-CyaA (red) monomers
522 followed by tryptophan fluorescence (s.d.: ± 1 nm). The variation of maximum wavelength
523 emission (λ_{max}) between CyaA and pro-CyaA is highlighted in panel D. Buffer: buffer A,
524 complemented with 2 mM $CaCl_2$. These experiments were performed in triplicate.

525

526 **Figure 3: HDX-MS analysis of CyaA refolding.** The structural organization of each domain
527 is displayed in Panel A and fits to the peptide maps shown in panels B, C and D. The 5 blocks
528 of RD are sized to fit to the peptide maps shown in panels B, C and D. The HDX-MS
529 behavior of CyaA in various concentrations of urea and in the presence of 2 mM calcium is
530 displayed in Panels B to D. At 6 M urea (B), no dynamic HDX-MS behavior is observed
531 throughout the protein. At 3 M urea (C), only RD and a small section of HR display dynamic
532 activity. At 1.6 M urea (D), the AC, HR and RD domains exhibit dynamic HDX-MS events.
533 Each dot corresponds to the average value of three independent replicates.

534

535 **Figure 4: Deuterium uptake differences of CyaA in urea in the presence and absence of**
536 **calcium.** The structural organization of each domain is displayed in Panel A and fits to the
537 peptide maps shown in panels B, C and D. The fractional uptake difference plots were
538 calculated at each urea concentration by subtracting the uptake measured in the absence (2
539 mM EDTA) and the presence of calcium (2 mM $CaCl_2$) for each peptide and at each time
540 point (Panels B-D). At 6 M urea, no difference of HDX-MS behavior is observed throughout
541 the protein. At 3 M urea (C), only RD displays significant positive difference of deuterium
542 uptake, indicative of a calcium-induced reduction of solvent accessibility, i.e., protein folding
543 in the presence of calcium. At 1.6 M urea (D), the AC, AR and RD domains show a positive
544 difference of deuterium uptake, indicating that the presence of calcium induces the folding of
545 these domains. Each dot corresponds to the average value of three independent replicates.

546

547 **Figure 5: Unique differences in HDX-MS behavior between pro-CyaA and CyaA in the**
548 **presence of calcium at 3 and 1.6 M urea.** The structural organization of each domain is
549 displayed in Panel A and fits to the peptide maps shown in panels B and C. Panels B-C
550 display the uptake difference plot between pro-CyaA and CyaA proteins at 3 M and 1.6 M
551 urea concentrations, respectively. Only a difference in HR was observed (highlighted in red
552 boxes). Each dot corresponds to the average value of three independent replicates. Panel C
553 shows peptides from HR with the greatest deuterium uptake differences between the two
554 proteins. Errors bars (SD) are within the size of the dots.

555
556 **Figure 6: HDX-MS analysis of monomeric pro-CyaA and CyaA species in solution.** The
557 structural organization of each domain is displayed in Panel A and fits to the peptide maps
558 shown in panels B, C and D. The HDX-MS behaviors of full-length pro-CyaA and CyaA
559 monomers measured in the presence of 2 mM calcium are given in Panels B and C. Dynamic
560 HDX-MS are observed throughout both proteins and over the time course of the reaction. The
561 uptake difference plot between both pro-CyaA and CyaA monomers is shown in Panel D.
562 Large differences in HDX-MS activity between the two proteins were observed in HR and
563 AR (red boxes). Smaller changes were found in T18, TR and Blocks I and II of RD. Each dot
564 corresponds to the average value of three independent replicates. Panel E shows selected
565 peptides from HR and AR. Errors bars (SD) are within the size of the dots.

566
567
568

569 **REFERENCES**

- 570 1. Siman, P., and Brik, A. (2012) Chemical and semisynthesis of posttranslationally
571 modified proteins. *Org Biomol Chem* **10**, 5684-5697
- 572 2. Ryslava, H., Doubnerova, V., Kavan, D., and Vanek, O. (2013) Effect of
573 posttranslational modifications on enzyme function and assembly. *J Proteomics*
574 **92**, 80-109
- 575 3. Linhartova, I., Bumba, L., Masin, J., Basler, M., Osicka, R., Kamanova, J.,
576 Prochazkova, K., Adkins, I., Hejnova-Holubova, J., Sadilkova, L., Morova, J., and
577 Sebo, P. (2010) RTX proteins: a highly diverse family secreted by a common
578 mechanism. *FEMS Microbiol Rev* **34**, 1076-1112
- 579 4. Chenal, A., Sotomayor Perez, A. C., and Ladant, D. (2015) Structure and function of
580 RTX Toxins. In *The Comprehensive Sourcebook of Bacterial Protein Toxins, 4th*
581 *Edition*, Elsevier
- 582 5. Issartel, J. P., Koronakis, V., and Hughes, C. (1991) Activation of Escherichia coli
583 prohaemolysin to the mature toxin by acyl carrier protein-dependent fatty
584 acylation. *Nature* **351**, 759-761
- 585 6. Welch, R. A. (1991) Pore-forming cytolysins of gram-negative bacteria. *Molecular*
586 *microbiology* **5**, 521-528
- 587 7. Hackett, M., Guo, L., Shabanowitz, J., Hunt, D. F., and Hewlett, E. L. (1994) Internal
588 lysine palmitoylation in adenylate cyclase toxin from Bordetella pertussis. *Science*
589 **266**, 433-435
- 590 8. Basar, T., Havlicek, V., Bezouskova, S., Hackett, M., and Sebo, P. (2001) Acylation
591 of lysine 983 is sufficient for toxin activity of Bordetella pertussis adenylate
592 cyclase. Substitutions of alanine 140 modulate acylation site selectivity of the
593 toxin acyltransferase CyaC. *J Biol Chem* **276**, 348-354
- 594 9. Greene, N. P., Crow, A., Hughes, C., and Koronakis, V. (2015) Structure of a
595 bacterial toxin-activating acyltransferase. *Proc Natl Acad Sci U S A* **112**, E3058-
596 3066
- 597 10. Fedele, G., Schiavoni, I., Adkins, I., Klimova, N., and Sebo, P. (2017) Invasion of
598 Dendritic Cells, Macrophages and Neutrophils by the Bordetella Adenylate
599 Cyclase Toxin: A Subversive Move to Fool Host Immunity. *Toxins (Basel)* **9**
- 600 11. Benz, R. (2016) Channel formation by RTX-toxins of pathogenic bacteria: Basis of
601 their biological activity. *Biochim Biophys Acta* **1858**, 526-537
- 602 12. Ladant, D., and Ullmann, A. (1999) Bordetella pertussis adenylate cyclase: a toxin
603 with multiple talents. *Trends in microbiology* **7**, 172-176
- 604 13. Vojtova, J., Kamanova, J., and Sebo, P. (2006) Bordetella adenylate cyclase toxin: a
605 swift saboteur of host defense. *Curr Opin Microbiol* **9**, 69-75
- 606 14. Guiso, N. (2017) Bordetella Adenylate Cyclase-Hemolysin Toxins. *Toxins (Basel)* **9**
- 607 15. Karst, J. C., Sotomayor Perez, A. C., Guijarro, J. I., Raynal, B., Chenal, A., and Ladant,
608 D. (2010) Calmodulin-induced conformational and hydrodynamic changes in the
609 catalytic domain of Bordetella pertussis adenylate cyclase toxin. *Biochemistry* **49**,
610 318-328
- 611 16. O'Brien, D. P., Durand, D., Voegelé, A., Hourdel, V., Davi, M., Chamot-Rooke, J.,
612 Vachette, P., Brier, S., Ladant, D., and Chenal, A. (2017) Calmodulin fishing with a
613 structurally disordered bait triggers CyaA catalysis. *PLoS Biol* **15**, e2004486
- 614 17. Carbonetti, N. H. (2010) Pertussis toxin and adenylate cyclase toxin: key
615 virulence factors of Bordetella pertussis and cell biology tools. *Future Microbiol* **5**,
616 455-469
- 617 18. Chenal, A., and Ladant, D. (2018) Bioengineering of Bordetella pertussis
618 Adenylate Cyclase Toxin for Antigen-Delivery and Immunotherapy. *Toxins (Basel)*
619 **10**

- 620 19. Glaser, P., Sakamoto, H., Bellalou, J., Ullmann, A., and Danchin, A. (1988) Secretion
621 of cyclolysin, the calmodulin-sensitive adenylate cyclase-haemolysin bifunctional
622 protein of *Bordetella pertussis*. *Embo J* **7**, 3997-4004
- 623 20. Bellalou, J., Sakamoto, H., Ladant, D., Geoffroy, C., and Ullmann, A. (1990)
624 Deletions affecting hemolytic and toxin activities of *Bordetella pertussis*
625 adenylate cyclase. *Infection and immunity* **58**, 3242-3247
- 626 21. Bellalou, J., Ladant, D., and Sakamoto, H. (1990) Synthesis and secretion of
627 *Bordetella pertussis* adenylate cyclase as a 200-kilodalton protein. *Infection and*
628 *immunity* **58**, 1195-1200
- 629 22. Sakamoto, H., Bellalou, J., Sebo, P., and Ladant, D. (1992) *Bordetella pertussis*
630 adenylate cyclase toxin. Structural and functional independence of the catalytic
631 and hemolytic activities. *J Biol Chem* **267**, 13598-13602
- 632 23. Martin, C., Requero, M. A., Masin, J., Konopasek, I., Goni, F. M., Sebo, P., and
633 Ostolaza, H. (2004) Membrane restructuring by *Bordetella pertussis* adenylate
634 cyclase toxin, a member of the RTX toxin family. *J Bacteriol* **186**, 3760-3765
- 635 24. Karst, J. C., Barker, R., Devi, U., Swann, M. J., Davi, M., Roser, S. J., Ladant, D., and
636 Chenal, A. (2012) Identification of a region that assists membrane insertion and
637 translocation of the catalytic domain of *Bordetella pertussis* CyaA toxin. *J Biol*
638 *Chem* **287**, 9200-9212
- 639 25. Masin, J., Osickova, A., Sukova, A., Fiser, R., Halada, P., Bumba, L., Linhartova, I.,
640 Osicka, R., and Sebo, P. (2016) Negatively charged residues of the segment linking
641 the enzyme and cytolysin moieties restrict the membrane-permeabilizing
642 capacity of adenylate cyclase toxin. *Sci Rep* **6**, 29137
- 643 26. Subrini, O., Sotomayor-Perez, A. C., Hessel, A., Spiaczka-Karst, J., Selwa, E., Sapay,
644 N., Veneziano, R., Pansieri, J., Chopineau, J., Ladant, D., and Chenal, A. (2013)
645 Characterization of a membrane-active peptide from the *Bordetella pertussis*
646 CyaA toxin. *J Biol Chem* **288**, 32585-32598
- 647 27. Voegele, A., Subrini, O., Sapay, N., Ladant, D., and Chenal, A. (2017) Membrane-
648 Active Properties of an Amphitropic Peptide from the CyaA Toxin Translocation
649 Region. *Toxins (Basel)* **9**
- 650 28. Barry, E. M., Weiss, A. A., Ehrmann, I. E., Gray, M. C., Hewlett, E. L., and Goodwin, M.
651 S. (1991) *Bordetella pertussis* adenylate cyclase toxin and hemolytic activities
652 require a second gene, *cyaC*, for activation. *J Bacteriol* **173**, 720-726
- 653 29. Masin, J., Basler, M., Knapp, O., El-Azami-El-Idrissi, M., Maier, E., Konopasek, I.,
654 Benz, R., Leclerc, C., and Sebo, P. (2005) Acylation of lysine 860 allows tight
655 binding and cytotoxicity of *Bordetella* adenylate cyclase on CD11b-expressing
656 cells. *Biochemistry* **44**, 12759-12766
- 657 30. Bouchez, V., Douche, T., Dazas, M., Delaplaine, S., Matondo, M., Chamot-Rooke, J.,
658 and Guiso, N. (2017) Characterization of Post-Translational Modifications and
659 Cytotoxic Properties of the Adenylate-Cyclase Hemolysin Produced by Various
660 *Bordetella pertussis* and *Bordetella parapertussis* Isolates. *Toxins (Basel)* **9**
- 661 31. Bauche, C., Chenal, A., Knapp, O., Bodenreider, C., Benz, R., Chaffotte, A., and
662 Ladant, D. (2006) Structural and functional characterization of an essential RTX
663 subdomain of *Bordetella pertussis* adenylate cyclase toxin. *J Biol Chem* **281**,
664 16914-16926
- 665 32. Chenal, A., Guijarro, J. I., Raynal, B., Delepierre, M., and Ladant, D. (2009) RTX
666 calcium binding motifs are intrinsically disordered in the absence of calcium:
667 implication for protein secretion. *J Biol Chem* **284**, 1781-1789
- 668 33. Sotomayor Perez, A. C., Karst, J. C., Davi, M., Guijarro, J. I., Ladant, D., and Chenal, A.
669 (2010) Characterization of the regions involved in the calcium-induced folding of

- 670 the intrinsically disordered RTX motifs from the bordetella pertussis adenylate
671 cyclase toxin. *Journal of molecular biology* **397**, 534-549
- 672 34. Chenal, A., Karst, J. C., Sotomayor Perez, A. C., Wozniak, A. K., Baron, B., England, P.,
673 and Ladant, D. (2010) Calcium-induced folding and stabilization of the
674 intrinsically disordered RTX domain of the CyaA toxin. *Biophys J* **99**, 3744-3753
- 675 35. Sotomayor-Perez, A. C., Ladant, D., and Chenal, A. (2011) Calcium-induced folding
676 of intrinsically disordered repeat-in-toxin (RTX) motifs via changes of protein
677 charges and oligomerization states. *J Biol Chem* **286**, 16997-17004
- 678 36. Sotomayor-Perez, A. C., Karst, J. C., Ladant, D., and Chenal, A. (2012) Mean net
679 charge of intrinsically disordered proteins: experimental determination of
680 protein valence by electrophoretic mobility measurements. *Methods in molecular
681 biology* **896**, 331-349
- 682 37. Sotomayor-Perez, A. C., Subrini, O., Hessel, A., Ladant, D., and Chenal, A. (2013)
683 Molecular Crowding Stabilizes Both the Intrinsically Disordered Calcium-Free
684 State and the Folded Calcium-Bound State of a Repeat in Toxin (RTX) Protein.
685 *Journal of the American Chemical Society* **135**, 11929-11934
- 686 38. Sotomayor-Perez, A. C., Ladant, D., and Chenal, A. (2015) Disorder-to-order
687 transition in the CyaA toxin RTX domain: implications for toxin secretion. *Toxins
688 (Basel)* **7**, 1-20
- 689 39. O'Brien, D. P., Hernandez, B., Durand, D., Hourdel, V., Sotomayor-Perez, A. C.,
690 Vachette, P., Ghomi, M., Chamot-Rooke, J., Ladant, D., Brier, S., and Chenal, A.
691 (2015) Structural models of intrinsically disordered and calcium-bound folded
692 states of a protein adapted for secretion. *Sci Rep* **5**, 14223
- 693 40. Bumba, L., Masin, J., Macek, P., Wald, T., Motlova, L., Bibova, I., Klimova, N.,
694 Bednarova, L., Veverka, V., Kachala, M., Svergun, D. I., Barinka, C., and Sebo, P.
695 (2016) Calcium-Driven Folding of RTX Domain beta-Rolls Ratchets Translocation
696 of RTX Proteins through Type I Secretion Ducts. *Mol Cell* **62**, 47-62
- 697 41. Cannella, S. E., Ntsogo Enguene, V. Y., Davi, M., Malosse, C., Sotomayor Perez, A. C.,
698 Chamot-Rooke, J., Vachette, P., Durand, D., Ladant, D., and Chenal, A. (2017)
699 Stability, structural and functional properties of a monomeric, calcium-loaded
700 adenylate cyclase toxin, CyaA, from *Bordetella pertussis*. *Sci Rep* **7**, 42065
- 701 42. O'Brien, D. P., Perez, A. C. S., Karst, J., Cannella, S. E., Enguene, V. Y. N., Hessel, A.,
702 Raoux-Barbot, D., Voegelé, A., Subrini, O., Davi, M., Guijarro, J. I., Raynal, B., Baron,
703 B., England, P., Hernandez, B., Ghomi, M., Hourdel, V., Malosse, C., Chamot-Rooke,
704 J., Vachette, P., Durand, D., Brier, S., Ladant, D., and Chenal, A. (2018) Calcium-
705 dependent disorder-to-order transitions are central to the secretion and folding
706 of the CyaA toxin of *Bordetella pertussis*, the causative agent of whooping cough.
707 *Toxicon : official journal of the International Society on Toxinology* **149**, 37-44
- 708 43. Rose, T., Sebo, P., Bellalou, J., and Ladant, D. (1995) Interaction of calcium with
709 *Bordetella pertussis* adenylate cyclase toxin. Characterization of multiple
710 calcium-binding sites and calcium-induced conformational changes. *J Biol Chem*
711 **270**, 26370-26376
- 712 44. Welch, R. A. (2001) RTX toxin structure and function: a story of numerous
713 anomalies and few analogies in toxin biology. *Current topics in microbiology and
714 immunology* **257**, 85-111
- 715 45. Veneziano, R., Rossi, C., Chenal, A., Devoisselle, J. M., Ladant, D., and Chopineau, J.
716 (2013) *Bordetella pertussis* adenylate cyclase toxin translocation across a
717 tethered lipid bilayer. *Proc Natl Acad Sci U S A* **110**, 20473-20478
- 718 46. Novak, J., Cerny, O., Osickova, A., Linhartova, I., Masin, J., Bumba, L., Sebo, P., and
719 Osicka, R. (2017) Structure-Function Relationships Underlying the Capacity of
720 *Bordetella Adenylate Cyclase Toxin to Disarm Host Phagocytes*. *Toxins (Basel)* **9**

- 721 47. Karst, J. C., Ntsogo Enguene, V. Y., Cannella, S. E., Subrini, O., Hessel, A., Debard, S.,
722 Ladant, D., and Chenal, A. (2014) Calcium, Acylation, and Molecular Confinement
723 Favor Folding of Bordetella pertussis Adenylate Cyclase CyaA Toxin into a
724 Monomeric and Cytotoxic Form. *J Biol Chem* **289**, 30702-30716
- 725 48. Cox, J., and Mann, M. (2008) MaxQuant enables high peptide identification rates,
726 individualized p.p.b.-range mass accuracies and proteome-wide protein
727 quantification. *Nature biotechnology* **26**, 1367-1372
- 728 49. Cox, J., Neuhauser, N., Michalski, A., Scheltema, R. A., Olsen, J. V., and Mann, M.
729 (2011) Andromeda: a peptide search engine integrated into the MaxQuant
730 environment. *J Proteome Res* **10**, 1794-1805
- 731 50. Hourdel, V., Volant, S., O'Brien, D. P., Chenal, A., Chamot-Rooke, J., Dillies, M. A.,
732 and Brier, S. (2016) MEMHDX: An interactive tool to expedite the statistical
733 validation and visualization of large HDX-MS datasets. *Bioinformatics (Oxford,*
734 *England)*
- 735 51. Karst, J. C., Sotomayor-Perez, A. C., Ladant, D., and Chenal, A. (2012) Estimation of
736 intrinsically disordered protein shape and time-averaged apparent hydration in
737 native conditions by a combination of hydrodynamic methods. *Methods in*
738 *molecular biology* **896**, 163-177
- 739 52. Karimova, G., Pidoux, J., Ullmann, A., and Ladant, D. (1998) A bacterial two-hybrid
740 system based on a reconstituted signal transduction pathway. *Proc Natl Acad Sci*
741 *U S A* **95**, 5752-5756
- 742 53. Sebo, P., Glaser, P., Sakamoto, H., and Ullmann, A. (1991) High-level synthesis of
743 active adenylate cyclase toxin of Bordetella pertussis in a reconstructed
744 Escherichia coli system. *Gene* **104**, 19-24
- 745 54. Westrop, G. D., Hormozi, E. K., Da Costa, N. A., Parton, R., and Coote, J. G. (1996)
746 Bordetella pertussis adenylate cyclase toxin: proCyaA and CyaC proteins
747 synthesised separately in Escherichia coli produce active toxin in vitro. *Gene* **180**,
748 91-99
- 749 55. Karimova, G., Fayolle, C., Gmira, S., Ullmann, A., Leclerc, C., and Ladant, D. (1998)
750 Charge-dependent translocation of Bordetella pertussis adenylate cyclase toxin
751 into eukaryotic cells: implication for the in vivo delivery of CD8(+) T cell epitopes
752 into antigen-presenting cells. *Proc Natl Acad Sci U S A* **95**, 12532-12537
- 753 56. Gmira, S., Karimova, G., and Ladant, D. (2001) Characterization of recombinant
754 Bordetella pertussis adenylate cyclase toxins carrying passenger proteins. *Res*
755 *Microbiol* **152**, 889-900
- 756 57. El-Azami-El-Idrissi, M., Bauche, C., Loucka, J., Osicka, R., Sebo, P., Ladant, D., and
757 Leclerc, C. (2003) Interaction of Bordetella pertussis adenylate cyclase with
758 CD11b/CD18: Role of toxin acylation and identification of the main integrin
759 interaction domain. *J Biol Chem* **278**, 38514-38521
- 760 58. Semisotnov, G. V., Rodionova, N. A., Razgulyaev, O. I., Uversky, V. N., Gripas, A. F.,
761 and Gilmanshin, R. I. (1991) Study of the "molten globule" intermediate state in
762 protein folding by a hydrophobic fluorescent probe. *Biopolymers* **31**, 119-128
- 763 59. O'Brien, D. P., Brier, S., Ladant, D., Durand, D., Chenal, A., and Vachette, P. (2018)
764 SEC-SAXS and HDX-MS: A powerful combination. The case of the calcium-binding
765 domain of a bacterial toxin. *Biotechnol Appl Biochem* **65**, 62-68
766

Figure 1

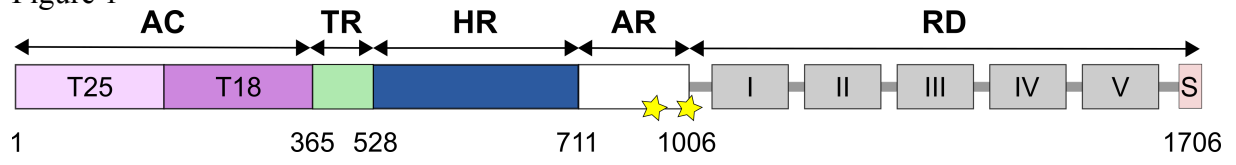


figure 2

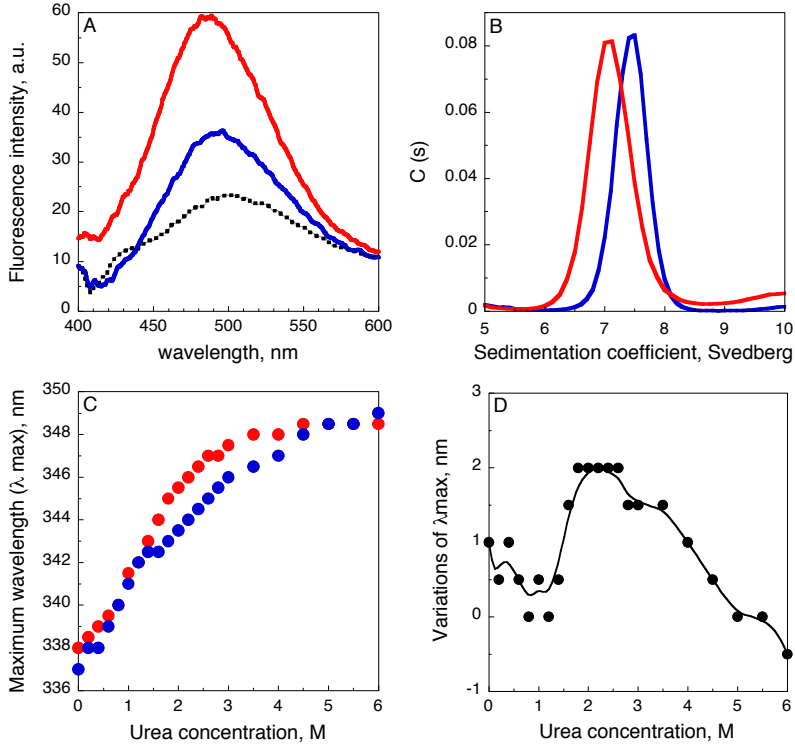


Figure 2

figure 3

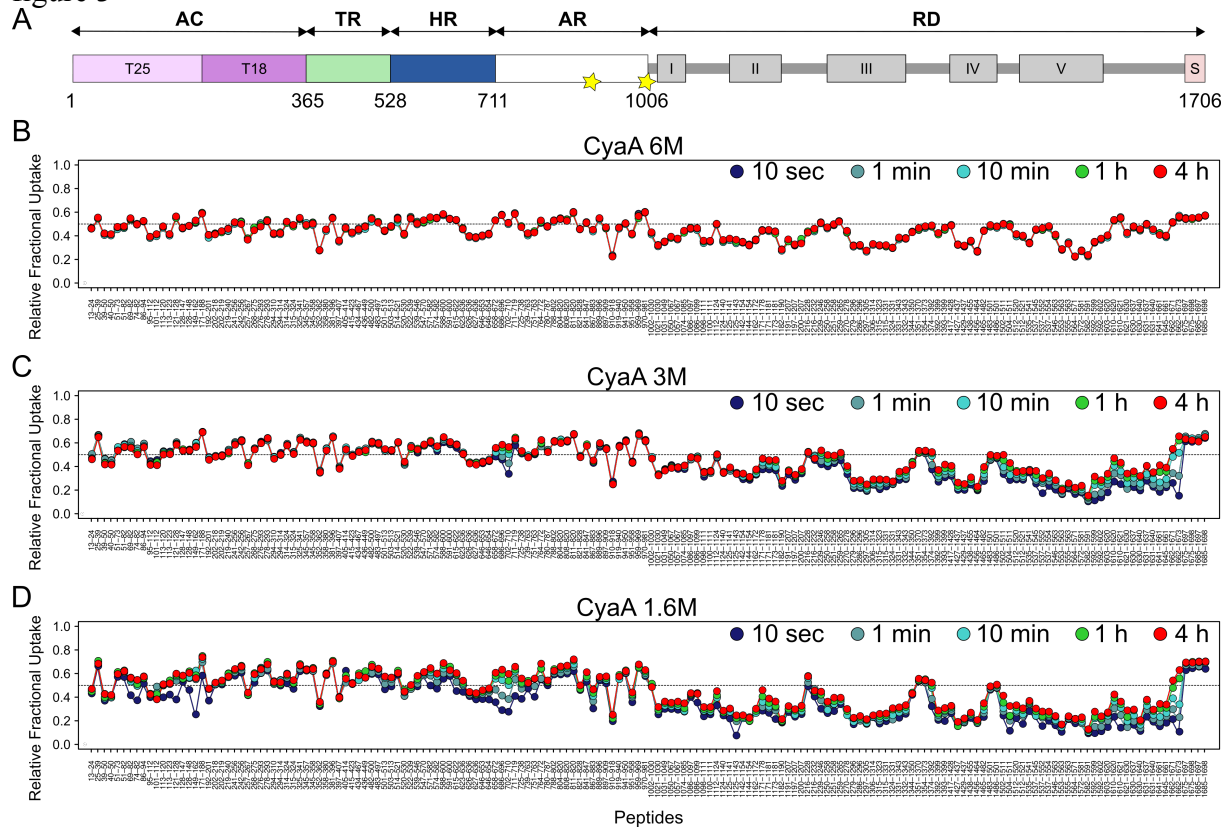


figure 4

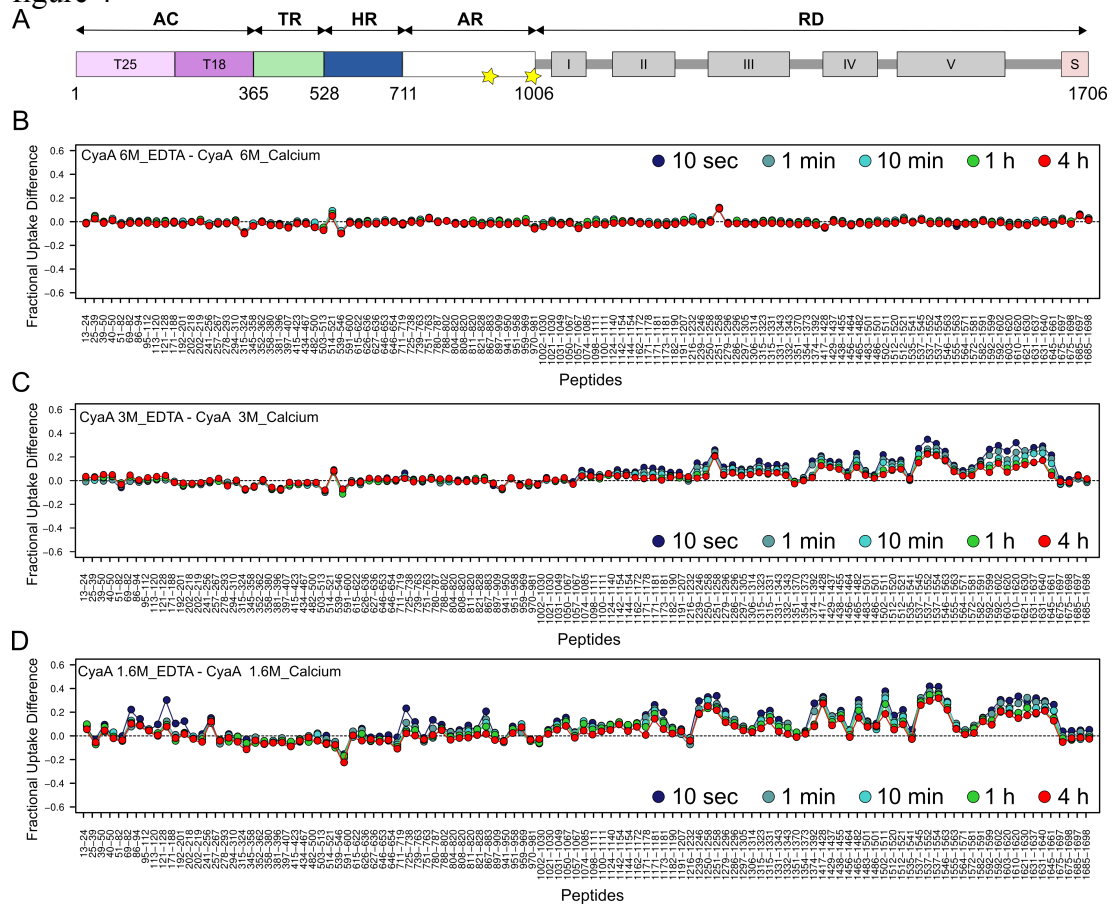


figure 5

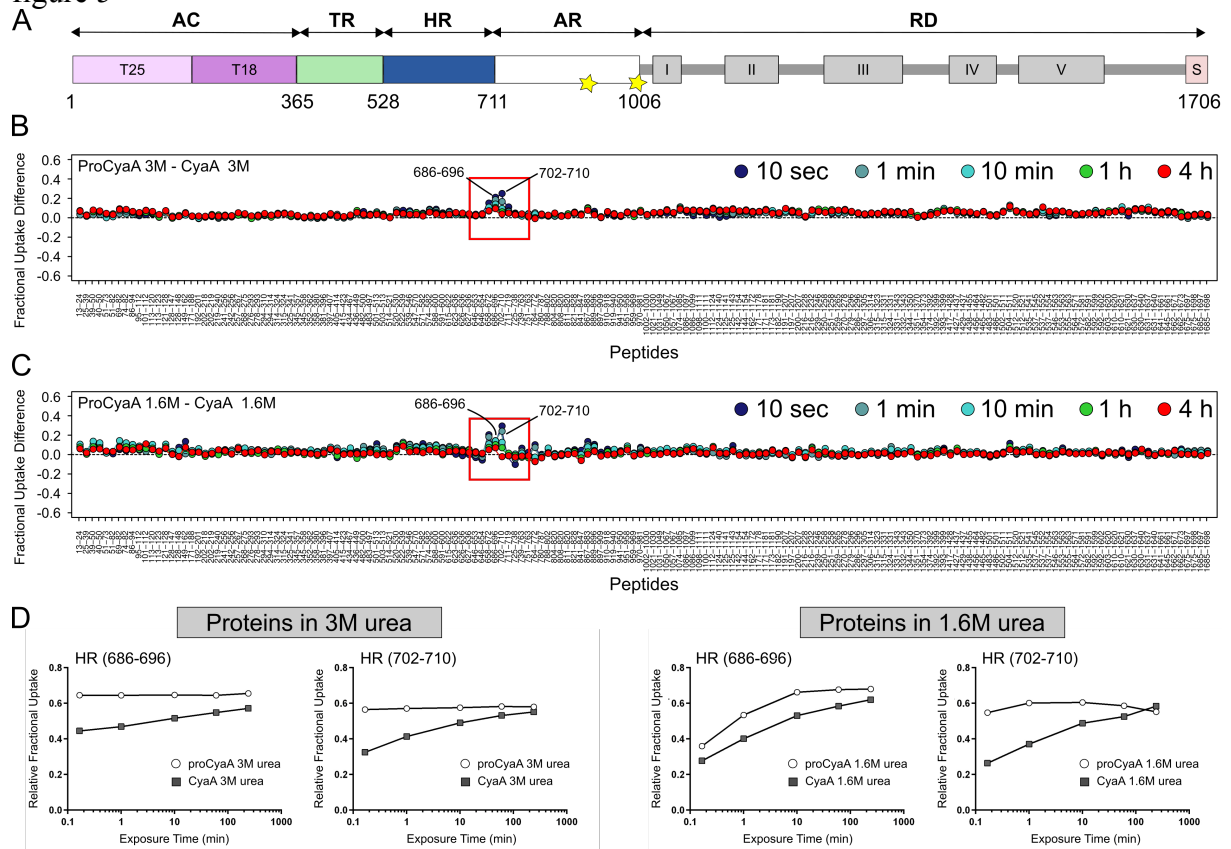


figure 6

